Spectral evidence for local-moment ferromagnetism in the van der Waals metals Fe_3GaTe_2 and Fe_3GeTe_2

Han Wu,[1] Chaowei Hu,[2,3] Yaofeng Xie,[1] Bo Gyu Jang,[4,5] Jianwei Huang,[1] Yucheng Guo,[1] Shan Wu,[6] Cheng Hu,[7] Ziqin Yue,[1] Yue Shi,[2] Rourav Basak,[8] Zheng Ren,[1] T. Yilmaz,[9] Elio Vescovo,[9] Chris Jozwiak,[7] Aaron Bostwick,[7] Eli Rotenberg,[7] Alexei Fedorov,[7] Jonathan D. Denlinger,[7] Christoph Klewe,[7] Padraic Shafer,[7] Donghui Lu,[10] Makoto Hashimoto,[10] Junichiro Kono,[11,1,12] Alex Frano,[8] Robert J. Birgeneau,[6,13,14] Xiaodong Xu,[2,3] Jian-Xin Zhu,[4] Pengcheng Dai,[1] Jiun-Haw Chu,[2] and Ming Yi[1,*]

[1]*Department of Physics and Astronomy and Rice Center for Quantum Materials, Rice University, Houston, Texas, 77005 USA*
[2]*Department of Physics, University of Washington, Seattle, Washington 98195, USA*
[3]*Department of Materials Science and Engineering, University of Washington, Seattle, Washington 98195, USA*
[4]*Theoretical Division and Center for Integrated Nanotechnologies, Los Alamos National Laboratory, Los Alamos, New Mexico, USA*
[5]*Department of Advanced Materials Engineering for Information and Electronics, Kyung Hee University, Yongin 17104, Republic of Korea*
[6]*Department of Physics, University of California at Berkeley, Berkeley, California 94720, USA*
[7]*Advanced Light Source, Lawrence Berkeley National Laboratory, Berkeley, California 94720, USA*
[8]*Department of Physics, University of California San Diego, La Jolla, California 92093,USA*
[9]*National Synchrotron Light Source II, Brookhaven National Lab, Upton, New York 11973, USA*
[10]*Stanford Synchrotron Radiation Lightsource, SLAC National Accelerator Laboratory, Menlo Park, California 94025, USA*
[11]*Department of Electrical and Computer Engineering, Rice University, Houston, Texas 77005, USA*
[12]*Department of Material Science and NanoEngineering, Rice University, Houston, Texas 77005, USA*
[13]*Materials Sciences Division, Lawrence Berkeley National Laboratory, Berkeley, California 94720, USA*
[14]*Department of Materials Science and Engineering, University of California, Berkeley, California,USA*

(Received 1 July 2023; revised 31 October 2023; accepted 20 February 2024; published 12 March 2024)

Magnetism in two-dimensional (2D) materials has attracted considerable attention recently for both fundamental understanding of magnetism and its tunability towards device applications. The isostructural Fe_3GeTe_2 and Fe_3GaTe_2 are two members of the Fe-based van der Waals (vdW) ferromagnet family, but exhibit very different Curie temperatures (T_C) of 210 and 360 K, respectively. Here, by using angle-resolved photoemission spectroscopy and density functional theory, we systematically compare the electronic structures of the two compounds. Qualitative similarities in the Fermi surface can be found between the two compounds, with expanded hole pockets in Fe_3GaTe_2 suggesting additional hole carriers compared to Fe_3GeTe_2. Interestingly, we observe almost no band shift in Fe_3GaTe_2 across its T_C of 360 K, compared to a small shift in Fe_3GeTe_2 across its T_C of 210 K. The weak temperature-dependent evolution strongly deviates from the expectations of an itinerant Stoner mechanism. Our results suggest that itinerant electrons have minimal contributions to the enhancement of T_C in Fe_3GaTe_2 compared to Fe_3GeTe_2, and that the nature of ferromagnetism in these Fe-based vdW ferromagnets must be understood with considerations of the electron correlations.

DOI: 10.1103/PhysRevB.109.104410

I. INTRODUCTION

The recently discovered van der Waals (vdW) family of ferromagnets exhibits Curie temperatures (T_C) ranging from 30 K to above room temperature [1–4]. The remarkable preservation of long-range ferromagnetic order in these materials in the two-dimensional (2D) regime position them as a promising class of materials for the development of next-generation spintronic devices [5–9]. Equally importantly, these vdW materials offer a new platform to probe 2D magnetism. Our understanding of magnetism has been developed from two opposing limits. One approach is based on the weak-coupling picture where ferromagnetism arises from spontaneous spin splitting of the itinerant electronic bands near the Fermi level (E_F) beginning at T_C [10–19], which can only occur in metals. The other approach is based on a strong-coupling picture where electrons are localized and magnetism arises from the Heisenberg exchange coupling of the local moments, where the magnetic exchange splitting has no temperature dependence across T_C, and is often associated with insulators [10,12,20–23]. In real materials, while the two limits exist, many compounds live in a regime where both mechanisms contribute. One such example is the iron-based superconductors (FeSCs) [24,25], where electron correlations are moderate in between the strongly localized Mott physics of the cuprates and the itinerant spin-density-wave chromium metal. Neutron scattering identifies itinerant spin excitations at low energies with large fluctuating moments up to high energies [26]. Even contradictory reports of

*mingyi@rice.edu

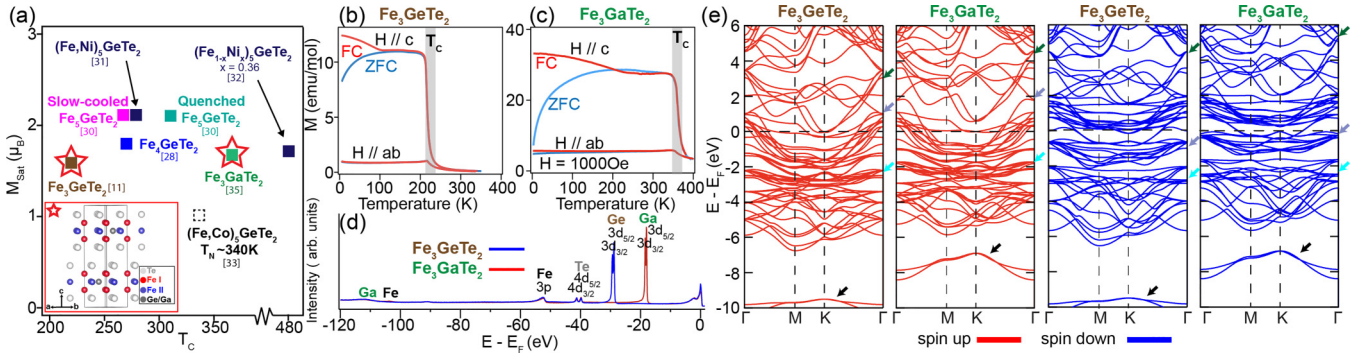

FIG. 1. (a) T_C and saturated moment (M_{sat}) comparison for reported Fe-based vdW magnets. All are ferromagnets except (Fe, Co)$_5$GeTe$_2$, which is an antiferromagnet. The inset shows the crystal structure for Fe_3XTe_2 (X = Ge, Ga). (b), (c) Temperature-dependent magnetization curves of Fe_3XTe_2. Zero-field-cooled (ZFC) and field-cooled (FC) curves indicate a ferromagnetic to paramagnetic transition at 210 K for Fe_3GeTe_2 and 360 K for Fe_3GaTe_2. (d) Core level photoemission spectra of Fe_3XTe_2. (e) DFT calculations for the ferromagnetic ground state, with the spin up and spin down bands indicated in red and blue, respectively. Spin-orbital coupling is not included. Pairs of arrows indicate the same features for comparison between the two compounds.

temperature-dependent exchange splitting have left a standing debate on the nature of magnetism in Fe and Ni metals [27].

The vdW ferromagnets can be largely grouped into two families, the insulating Cr-based compounds such as $Cr_2Ge_2Te_6$ [1,28] and CrI_3 [2], and the metallic Fe-based compounds such as Fe_nXTe_2 ($n = 3$–5; X = Ge, Ga) (FGTs) [29]. The ferromagnetism in the insulating Cr-based compounds indeed can be understood by an anisotropic Heisenberg model where correlations between local moments persist to well above T_C [20,21]. As a result, the electronic structure only exhibits very subtle evolution across T_C [30] while the FGTs are quite different. Consisting of Te-sandwiched vdW slabs, the various members of this family differ structurally in the number of Fe sites within each slab as well as the number of slabs within a unit cell dictated by the stacking order [7,31–39]. Notably, the T_C's of the FGTs are close to or even above room temperature [Fig. 1(a)] [7,31–37]. As metals, the FGTs are often referred to as itinerant magnets. However, ample evidence suggest a coexistence of both local moments and itinerant electrons. $Fe_{3-x}GeTe_2$ with a T_C that varies between 140 to 220 K [3,4], in particular, has been demonstrated by neutron scattering to exhibit a dual nature of magnetic excitations [40]. Angle-resolved photoemission spectroscopy (ARPES) measurements indicate a deviation from Stone-type spin splitting across T_C as well as spectral weight transfer suggestive of Kondo behavior [11,41–44]. Very recently, Fe_3GaTe_2, isostructural to Fe_3GeTe_2, has been synthesized and shown to exhibit a remarkable above-room temperature T_C of 360 K, along with a high saturation magnetic moment, significant perpendicular magnetic anisotropy energy density, and a large anomalous Hall angle at room temperature [39,45–48]. These findings highlight the potential of Fe_3GaTe_2 as an exciting material for applications. The identical crystal structure but drastically different T_C's in these two compounds offer an opportunity to probe into the nature of the magnetism in these materials. Here, via systematic ARPES measurements and density functional theory calculations, we compare and contrast the electronic structure of Fe_3GaTe_2 and Fe_3GeTe_2. We find Fe_3GaTe_2 to be an effectively hole-doped version of Fe_3GeTe_2. In a large energy range of the valence bands, we identify a separation of the spectral weight that seems to be consistent with the predicted Fe spin up and spin down states. However, we find no observable shift in the electronic structures of Fe_3GaTe_2 across its T_C, compared to a subtle shift for Fe_3GeTe_2. Taken all together, the origins of magnetism in both Fe_3GaTe_2 and Fe_3GeTe_2 deviate strongly from the expectations of the itinerant Stoner model, with Fe_3GaTe_2 exhibiting an even stronger local moment behavior. Our results indicate that the local moments are crucial for explaining the nature of ferromagnetism in FGTs, and are likely responsible for the much enhanced T_C in Fe_3GaTe_2.

II. RESULTS AND DISCUSSION

High-quality Fe_3GaTe_2 and Fe_3GeTe_2 single crystals were synthesized by a chemical transport method [40]. ARPES measurements were carried out at beamline 5-2 of the Stanford Synchrotron Radiation Lightsource, ESM (21ID-I) beamline of the National Synchrotron Light Source II, and beamlines 7.0.2.1, 10.0.1, and 4.0.3 of the Advanced Light Source, using DA30, DA30, R4000, and R8000 electron analyzers, respectively. The overall energy and angular resolutions were 15 meV and 0.1°, respectively. All data shown in the main text were taken with 132 eV photons, with additional photon energy-dependence data shown in the Supplemental Material (SM) [49]. All data were taken at 15 K unless otherwise noted. The DFT calculations were carried out by using WIEN2K package which uses the full-potential augmented plane wave plus local orbital as the basis [50]. The Perdew-Burke-Ernzefhof (PBE) generalized gradient approximation (GGA) was employed for the exchange-correlation functional [51] and a $16 \times 16 \times 3$ k-point mesh for self-consistent calculation.

As depicted in Fig. 1(a), Fe_3XTe_2 has a layered hexagonal crystal structure in the space group $P63/mmc$ (No. 194) [52]. The lattice parameter for Fe_3GaTe_2 ($a = 4.07$ Å, $c = 16.1$ Å) and Fe_3GeTe_2 ($a = 3.99$ Å, $c = 16.3$ Å) are similar, as previously reported [39,52]. The unit cell consists of two vdW slabs, each with two nonequivalent Fe sites, Fe I and Fe II, and has the symmetry operators C_{3z}, C_{2y} and P (inversion) that enforce the emergence of topological nodal lines in the presence of ferromagnetism, giving rise to a tunable intrinsic

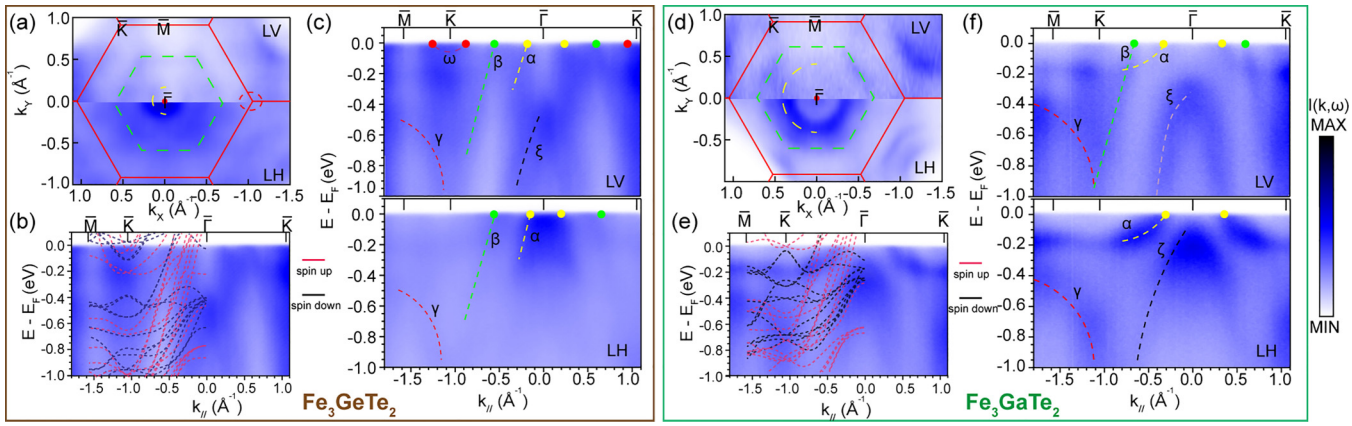

FIG. 2. (a) Fermi surface mapping with LH and LV polarized light for Fe_3GeTe_2, with BZ boundaries labeled by red lines. (b) Measured dispersions along the $\overline{M}$-$\overline{K}$-$\overline{\Gamma}$-$\overline{K}$ direction overlaid with DFT calculations that are renormalized by a factor of 1.6. (c) LV and LH polarization dependent dispersions measured along the $\overline{M}$-$\overline{K}$-$\overline{\Gamma}$-$\overline{K}$ direction, with key features marked by dashed lines. (d)–(f) Same measurements as (a)–(c) but for Fe_3GaTe_2.

anomalous Hall current [52,53]. Our DFT calculations for the ferromagnetic FM phase of both compounds are shown in Fig. 1(e), where the topological crossings at the K point can be seen. The zero-field-cooled (ZFC) and field-cooled (FC) magnetization measurements [Figs. 1(b) and 1(c)] for the two compounds show a T_C of 210 K for Fe_3GeTe_2 and 360 K for Fe_3GaTe_2, in agreement with previous reports [3,4,11,39,42]. From a comparison of our DFT calculations for the ferromagnetic ground state, Fe_3GaTe_2 is an effective hole-doped version of Fe_3GeTe_2, as the band structure is qualitatively similar except a shifting down of the chemical potential in Fe_3GaTe_2 [Fig. 1(e)].

First, we show in Fig. 1(d) the integrated core-level photoemission spectrum of the two compounds. We also observe clear x-ray magnetic circular dichroism signal at the Fe L edge for both compounds (see SM [49]). As expected, the core level spectra for the two compounds are very similar except the distinct Ge and Ga 3d peaks. Next, we present the electronic structure of the ferromagnetic phase of Fe_3GaTe_2 and Fe_3GeTe_2 as measured by ARPES. The electronic structure of the two compounds near E_F are compared in Fig. 2, as measured by both linear vertical (LV) and linear horizontal (LH) polarized light. Consistent with previous reports on Fe_3GeTe_2 [11], we observe two hole Fermi pockets centered at the $\overline{\Gamma}$ point: an inner circular pocket and an outer hexagonal pocket [Fig. 2(a)]. They are formed by two dispersive bands as observed on the high symmetry cut, and we label them as the α and β bands [Fig. 2(c)]. Additionally, a small electron pocket is observed at the $\overline{K}$ point, which we label as the ω band. From the high symmetry cut, we also observe two other dispersions that do not cross E_F, which we label the ξ and γ bands. For Fe_3GaTe_2, we also observe two hole Fermi pockets at the $\overline{\Gamma}$ point [Fig. 2(d)], both with similar shapes but expanded areas as compared to those in Fe_3GeTe_2, indicating additional hole charge carriers in Fe_3GaTe_2 compared to Fe_3GeTe_2. From the high symmetry cut [Fig. 2(f), both the inner α band and the outer β band appear to cross E_F at larger Fermi momenta. The γ band is also observed to shift up in energy compared to that in Fe_3GeTe_2. When we compare the near-E_F measured dispersions with those by DFT calculations, we find that a renormalization factor of 1.6 can achieve a reasonable agreement for both compounds [Figs. 2(b) and 2(e)], including the locations of the hole band tops at $\overline{\Gamma}$ (see SM for discussion [49]). The renormalization factor is consistent with that determined for Fe_3GeTe_2 previously [11], and is slightly larger than that for Fe metal [54,55].

Having examined the electronic structure in the near E_F region, we next present the spectra in the large energy range covering the entire valence bands. Figures 3(a) and 3(b) show the spectra within 6 eV below E_F along the $\overline{M}$-$\overline{K}$-$\overline{\Gamma}$ high symmetry direction for both compounds. Visibly, the spectrum is separated into sharp dispersions within 1 eV of E_F and broad spectral intensity in the -2 to -3 eV energy range. As shown in Figs. 3(a) and 3(b), the sharp dispersions marked by the solid lines and the broad spectral intensity indicated by dashed lines exhibit similar dispersion patterns. This is also clearly shown in the stack of energy distribution curves (EDCs) in Figs. 3(c) and 3(d). The broad hump (green markers) largely follows the dispersion and photoemission matrix elements of the sharper bands near E_F (yellow markers), and a clear dip (red arrows) separates the two regimes of sharp quasiparticles and broad spectral weight. Even in this large energy window, it is evident that the overall spectral shape of Fe_3GaTe_2 is shifted up in energy compared to that of Fe_3GeTe_2, consistent with the overall hole doping. To understand the origin of these states, we look at the DFT calculated density of states (DOS) in the ferromagnetic state. Clearly, Fe 3d states dominate the valence bands, with a small contribution by Te and Ge/Ga. To take into consideration the renormalization of the Fe 3d states derived above, we renormalize the Fe partial DOS by 1.6 while leaving the Te and Ge/Ga partial DOS unrenormalized. This results in the spin majority (up) states having a peak near -2 eV and the spin minority (down) states near E_F. This comparison suggests that the sharper quasiparticles and broad hump dichotomy is likely dominated by the spin minority and spin majority states, respectively. This kind of quasiparticle–dip–broad-hump spectral feature has also been reported in other correlated ferromagnets, such as $SrRuO_3$, which is a metallic ferromagnet where both itinerant electrons and local moments contribute to the magnetism. In

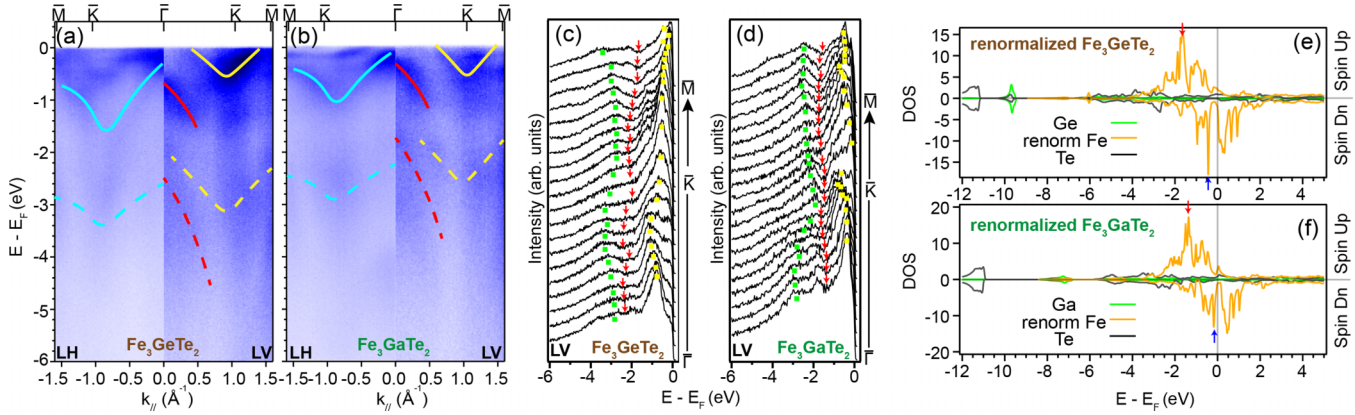

FIG. 3. (a), (b) Large energy range spectra under both LH and LV polarizations for Fe_3GeTe_2 and Fe_3GaTe_2. The solid lines highlight the coherent features near E_F and the dashed lines highlight the corresponding incoherent features. (c), (d) EDCs along the $\overline{M}$-$\overline{K}$-$\overline{\Gamma}$ directions for the LV polarization from (a), (b). The green dots track the incoherent peaks and the yellow dots track the coherent peaks. The two features are separated by the dips that marked with red arrows. (e), (f) Projected partial DOS calculated by DFT for Fe_3GeTe_2 and Fe_3GaTe_2. Only the Fe partial DOS is renormalized by a factor of 1.6. The arrows are pointing at the same features in Fe_3GaTe_2 and Fe_3GeTe_2, suggesting that Fe_3GaTe_2 is a hole-doped version of Fe_3GeTe_2.

that case, this quasiparticle–dip–broad-hump spectral feature was also explicitly reported, where strong scattering results in the incoherence of the spin majority states [56,57]. In Fe and Ni metals, the local density approximation (LDA) plus dynamical mean field theory has also captured such a spectral line shape in the single-particle spectral function by including the many-body effects of the 3*d* states [42,54,58].

To examine the role of the near-E_F bands in the ferromagnetism, we carried out a temperature dependence study of the electronic structures for both Fe_3GaTe_2 and Fe_3GeTe_2 across their respective T_C. Figure 4(a) shows the band dispersions of Fe_3GeTe_2 ($T_C = 210$ K) at 50 and 250 K, with additional intermediate temperatures shown in the SM [49]. And Fig. 4(b) displays the band dispersion of Fe_3GaTe_2 ($T_C = 360$ K) along the $\overline{M}$-$\overline{K}$-$\overline{\Gamma}$ direction at selected temperatures 50 and 410 K, with additional intermediate temperatures shown in the SM [49]. From those datasets, we can extract the temperature evolution of the bands by extracting the EDCs at specific momenta indicated by the orange and green lines in Figs. 4(a) and 4(b). The detailed EDCs are shown in Figs. 4(c) and 4(f). For Fe_3GeTe_2, the β band is observed to not shift; a small shift of the ξ band is observed across T_C, consistent with previous report [11]. Similar analysis was also carried out for Fe_3GaTe_2. And for Fe_3GaTe_2, there is no noticeable shift in the peak position of the EDCs for both α and ζ bands with increasing temperature through the T_C of 360 K, as shown also from the fitted peak positions in Fig. 4(g). The lack of observable shift of bands across T_C strongly deviates from the expected behavior of itinerant ferromagnets. According to the Stoner model, the exchange splitting is expected to disappear above T_C [59]. For Fe_3GeTe_2 and Fe_3GaTe_2, we can estimate the exchange splitting sizes from DFT calculations to be approximately 1.5 and 1.7 eV, respectively. The expected shift of majority/minority bands would be half of the

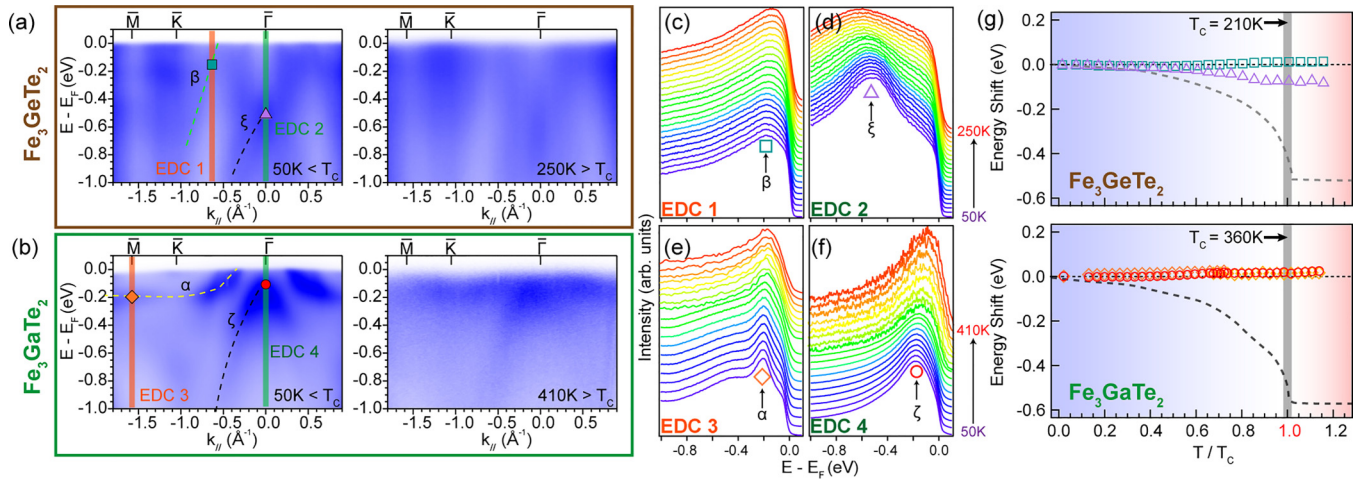

FIG. 4. (a), (b) Band dispersions in Fe_3GeTe_2 and Fe_3GaTe_2 above and below their respective T_C's. The main features are highlighted with dashed lines. (c)–(f) Temperature dependent EDCs, taken at the momenta marked in (a), (b). (g) Fitted peak positions from the EDCs as a function of temperature, with the markers defined as in (c)–(f). The grey dashed lines indicate the estimated band shift from a Stoner model, determined by the DFT exchange splitting and magnetic moment for Fe_3GeTe_2 [11] and magnetization for Fe_3GaTe_2 [39].

exchange splitting divided by the band renormalization factors, resulting in 0.47 and 0.53 eV, respectively. The temperature evolution of the band shift according to the Stoner model can then be estimated by scaling this energy scale to the existing temperature-dependent bulk magnetization in Fe_3GaTe_2 [39] or magnetic moment measured by neutron diffraction for Fe_3GeTe_2 [11,39], which are plotted as the grey dashed lines in Fig. 4(g). We note that for systems whose ferromagnetism is contributed by both itinerant electrons and local moments, partial closing of the exchange splitting is observed across T_C, such as Fe metal [60,61], MnSi [62,63], and $SrRuO_3$ [56,57]. The stark contrast between the expected shift and the observed band shift here suggests that itinerant electrons play a minimal role in the ferromagnetism in Fe_3GeTe_2 and Fe_3GaTe_2. While some finite shift is still observed in Fe_3GeTe_2, we observe no shift in Fe_3GaTe_2, suggesting that local moments play an even more dominant role in Fe_3GaTe_2.

III. CONCLUSION

Taking all the presented evidence together, we come to an understanding of the ferromagnetism of the isostructural Fe_3GaTe_2 ($T_C \sim 360$ K) and Fe_3GeTe_2 ($T_C \sim 210$ K) as the following: while both systems are metallic and exhibit clear Fermi surfaces, the valence band spectral intensity exhibits a quasiparticle–dip–broad-hump feature that seem to indicate non-negligible correlation effects. In addition, the itinerant charge carriers near E_F show minimal modifications across T_C, with Fe_3GaTe_2 showing even less observable changes. This indicates that the large enhancement of T_C in Fe_3GaTe_2 cannot be due to only the change in the itinerant charge carriers and must be a result of the local moments. Our findings therefore demonstrate that the Fe_3GaTe_2 and Fe_3GeTe_2 systems are moderately correlated, and a comprehensive understanding of the magnetism in these Fe-based vdW ferromagnets must take into consideration the many-body interactions of the Fe 3*d* states.

ACKNOWLEDGMENTS

This research used resources of the Advanced Light Source and the Stanford Synchrotron Radiation Lightsource, both U.S. Department Of Energy (DOE) Office of Science User Facilities under Contracts No. DE-AC02-05CH11231 and No. AC02-76SF00515, respectively. ARPES work is supported by the U.S. DOE Grant No. DE-SC0021421, the Gordon and Betty Moore Foundation's EPiQS Initiative through Grant No. GBMF9470. Y.C.G. is supported by the Robert A. Welch Foundation, Grant No. C-2175 (M.Y.). The sample growth efforts at Rice are supported by the U.S. DOE, BES under Grant No. DE-SC0012311 and the Robert A. Welch Foundation under Grant No. C-1839 (P.D.). Work at University of California, Berkeley, is funded by the U.S. Department of Energy, Office of Science, Office of Basic Energy Sciences, Materials Sciences and Engineering Division under Contract No. DE-AC02-05-CH11231 (Quantum Materials program KC2202). Work at Los Alamos was carried out under the auspices of the U.S. Department of Energy (DOE) National Nuclear Security Administration (NNSA) under Contract No. 89233218CNA000001, and was supported by the LANL LDRD Program and in part by Center for Integrated Nanotechnologies, a DOE BES user facility, in partnership with the LANL Institutional Computing Program for computational resources. Materials synthesis at UW was supported as part of Programmable Quantum Materials, an Energy Frontier Research Center funded by the U.S. Department of Energy (DOE), Office of Science, Basic Energy Sciences (BES), under Award No. DE-SC0019443.

[1] C. Gong, L. Li, Z. Li, H. Ji, A. Stern, Y. Xia, T. Cao, W. Bao, C. Wang, Y. Wang, Z. Q. Qiu, R. J. Cava, S. G. Louie, J. Xia, and X. Zhang, Discovery of intrinsic ferromagnetism in two-dimensional van der Waals crystals, Nature (London) **546**, 265 (2017).

[2] B. Huang, G. Clark, E. Navarro-Moratalla, D. R. Klein, R. Cheng, K. L. Seyler, D. Zhong, E. Schmidgall, M. A. McGuire, D. H. Cobden, W. Yao, D. Xiao, P. Jarillo-Herrero, and X. Xu, Layer-dependent ferromagnetism in a van der Waals crystal down to the monolayer limit, Nature (London) **546**, 270 (2017).

[3] Y. Deng, Y. Yu, Y. Song, J. Zhang, N. Z. Wang, Z. Sun, Y. Yi, Y. Z. Wu, S. Wu, J. Zhu, J. Wang, X. H. Chen, and Y. Zhang, Gate-tunable room-temperature ferromagnetism in two-dimensional Fe_3GeTe_2, Nature (London) **563**, 94 (2018).

[4] Z. Fei, B. Huang, P. Malinowski, W. Wang, T. Song, J. Sanchez, W. Yao, D. Xiao, X. Zhu, A. F. May, W. Wu, D. H. Cobden, J.-H. Chu, and X. Xu, Two-dimensional itinerant ferromagnetism in atomically thin Fe_3GeTe_2, Nat. Mater. **17**, 778 (2018).

[5] K. Yamada, C. H. Lee, K. Kurahashi, J. Wada, S. Wakimoto, S. Ueki, H. Kimura, Y. Endoh, S. Hosoya, G. Shirane, R. J. Birgeneau, M. Greven, M. A. Kastner, and Y. J. Kim, Doping dependence of the spatially modulated dynamical spin correlations and the superconducting-transition temperature in $La_{2-x}Sr_xCuO_4$, Phys. Rev. B **57**, 6165 (1998).

[6] K. S. Burch, D. Mandrus, and J.-G. Park, Magnetism in two-dimensional van der Waals materials, Nature (London) **563**, 47 (2018).

[7] C. Gong and X. Zhang, Two-dimensional magnetic crystals and emergent heterostructure devices, Science **363**, eaav4450 (2019).

[8] K. F. Mak, J. Shan, and D. C. Ralph, Probing and controlling magnetic states in 2D layered magnetic materials, Nat. Rev. Phys. **1**, 646 (2019).

[9] M. Gibertini, M. Koperski, A. F. Morpurgo, and K. S. Novoselov, Magnetic 2D materials and heterostructures, Nat. Nanotechnol. **14**, 408 (2019).

[10] S. Schmitt, N. Grewe, and T. Jabben, Itinerant and local-moment magnetism in strongly correlated electron systems, Phys. Rev. B **85**, 024404 (2012).

[11] X. Xu, Y. W. Li, S. R. Duan, S. L. Zhang, Y. J. Chen, L. Kang, A. J. Liang, C. Chen, W. Xia, Y. Xu, P. Malinowski, X. D. Xu, J.-H. Chu, G. Li, Y. F. Guo, Z. K. Liu, L. X. Yang, and Y. L. Chen, Signature for non-stoner ferromagnetism in the van

der Waals ferromagnet Fe_3GeTe_2, Phys. Rev. B **101**, 201104 (2020).
[12] M. D. Vannette, S. L. Bud'ko, P. C. Canfield, and R. Prozorov, Distinguishing local moment versus itinerant ferromagnets: Dynamic magnetic susceptibility, J. Appl. Phys. **103**, 07D302 (2008).
[13] E. C. Stoner, Collective electron ferromagnetism, Proc. R. Soc. Lond. A **165**, 372 (1938).
[14] S. V. Dordevic, D. N. Basov, N. R. Dilley, E. D. Bauer, and M. B. Maple, Hybridization gap in heavy fermion compounds, Phys. Rev. Lett. **86**, 684 (2001).
[15] T. Moriya, Recent progress in the theory of itinerant electron magnetism, J. Magn. Magn. Mater. **14**, 1 (1979).
[16] F. Bloch, Bemerkung zur elektronentheorie des ferromagnetismus und der elektrischen leitfähigkeit, Z. Phys. **57**, 545 (1929).
[17] J. C. Slater, The ferromagnetism of nickel, Phys. Rev. **49**, 537 (1936).
[18] C. Edmund and F. R. Stoner, Ferromagnetism, Rep. Prog. Phys. **11**, 43 (1947).
[19] X.-F. Su, Z.-L. Gu, Z.-Y. Dong, S.-L. Yu, and J.-X. Li, Ferromagnetism and spin excitations in topological Hubbard models with a flat band, Phys. Rev. B **99**, 014407 (2019).
[20] T. J. Williams, A. A. Aczel, M. D. Lumsden, S. E. Nagler, M. B. Stone, J.-Q. Yan, and D. Mandrus, Magnetic correlations in the quasi-two-dimensional semiconducting ferromagnet $CrSiTe_3$, Phys. Rev. B **92**, 144404 (2015).
[21] L. Chen, C. Mao, J.-H. Chung, M. B. Stone, A. I. Kolesnikov, X. Wang, N. Murai, B. Gao, O. Delaire, and P. Dai, Anisotropic magnon damping by zero-temperature quantum fluctuations in ferromagnetic $CrGeTe_3$, Nat. Commun. **13**, 4037 (2022).
[22] J. B. Goodenough, Narrow-band electrons in transition-metal oxides, Czech. J. Phys. **17**, 304 (1967).
[23] W. Heisenberg, Zur theorie des ferromagnetismus, Z. Physik **49**, 619 (1928).
[24] M. Yi, H. Pfau, Y. Zhang, Y. He, H. Wu, T. Chen, Z. R. Ye, M. Hashimoto, R. Yu, Q. Si, D.-H. Lee, P. Dai, Z.-X. Shen, D. H. Lu, and R. J. Birgeneau, Nematic energy scale and the missing electron pocket in FeSe, Phys. Rev. X **9**, 041049 (2019).
[25] J. Huang, R. Yu, Z. Xu, J.-X. Zhu, J. S. Oh, Q. Jiang, M. Wang, H. Wu, T. Chen, J. D. Denlinger, S.-K. Mo, M. Hashimoto, M. Michiardi, T. M. Pedersen, S. Gorovikov, S. Zhdanovich, A. Damascelli, G. Gu, P. Dai, J.-H. Chu, D. Lu, Q. Si, R. J. Birgeneau, and M. Yi, Correlation-driven electronic reconstruction in $FeTe_{1-x}Se_x$, Commun. Phys. **5**, 29 (2022).
[26] P. Dai, Antiferromagnetic order and spin dynamics in iron-based superconductors, Rev. Mod. Phys. **87**, 855 (2015).
[27] D. E. Eastman, F. J. Himpsel, and J. A. Knapp, Experimental band structure and temperature-dependent magnetic exchange splitting of nickel using angle-resolved photoemission, Phys. Rev. Lett. **40**, 1514 (1978).
[28] H. Wu, J.-X. Zhu, L. Chen, M. W. Butcher, Z. Yue, D. Yuan, Y. He, J. S. Oh, B. Gao, J. Huang, S. Wu, C. Gong, Y. Guo, S.-K. Mo, J. Denlinger, D. Lu, M. Hashimoto, M. B. Stone, A. I. Kolesnikov, S. Chi, J. Kono, A. H. Nevidomskyy, R. J. Birgeneau, P. Dai, and M. Yi, Two-step electronic response to magnetic ordering in a van der Waals ferromagnet, Phys. Rev. B **109**, 045416 (2024).
[29] H. Wu, L. Chen, P. Malinowski, J. Huang, Q. Deng, K. Scott, B. G. Jang, J. P. C. Ruff, Y. He, X. Chen, C. Hu, Z. Yue, J. S. Oh, X. Teng, Y. Guo, M. Klemm, C. Shi, Y. Shi, C. Setty, T. Werner, M. Hashimoto, D. Lu, T. Yilmaz, E. Vescovo, S.-K. Mo, A. Fedorov, J. Denlinger, Y. Xie, B. Gao, J. Kono, P. Dai, Y. Han, X. Xu, R. J. Birgeneau, J.-X. Zhu, E. H. da Silva Neto, L. Wu, J.-H. Chu, Q. Si, and M. Yi, Reversible non-volatile electronic switching in a near room temperature van der Waals ferromagnet, arXiv:2307.03154.
[30] M. D. Watson, I. Marković, F. Mazzola, A. Rajan, E. A. Morales, D. M. Burn, T. Hesjedal, G. van der Laan, S. Mukherjee, T. K. Kim, C. Bigi, I. Vobornik, M. C. Hatnean, G. Balakrishnan, and P. D. C. King, Direct observation of the energy gain underpinning ferromagnetic superexchange in the electronic structure of $CrGeTe_3$, Phys. Rev. B **101**, 205125 (2020).
[31] B. Chen, J. Yang, H. Wang, M. Imai, H. Ohta, C. Michioka, K. Yoshimura, and M. Fang, Magnetic properties of layered itinerant electron ferromagnet Fe_3GeTe_2, J. Phys. Soc. Jpn. **82**, 124711 (2013).
[32] J. Seo, D. Y. Kim, E. S. An, K. Kim, G.-Y. Kim, S.-Y. Hwang, D. W. Kim, B. G. Jang, H. Kim, G. Eom, S. Y. Seo, R. Stania, M. Muntwiler, J. Lee, K. Watanabe, T. Taniguchi, Y. J. Jo, J. Lee, B. I. Min, M. H. Jo, H. W. Yeom, S.-Y. Choi, J. H. Shim, and J. S. Kim, Nearly room temperature ferromagnetism in a magnetic metal-rich van der Waals metal, Sci. Adv. **6**, eaay8912 (2020).
[33] H. Zhang, R. Chen, K. Zhai, X. Chen, L. Caretta, X. Huang, R. V. Chopdekar, J. Cao, J. Sun, J. Yao, R. Birgeneau, and R. Ramesh, Itinerant ferromagnetism in van der Waals $Fe_{5-x}GeTe_2$ crystals above room temperature, Phys. Rev. B **102**, 064417 (2020).
[34] A. F. May, C. A. Bridges, and M. A. McGuire, Physical properties and thermal stability of $Fe_{5-x}GeTe_2$ single crystals, Phys. Rev. Mater. **3**, 104401 (2019).
[35] J. Stahl, E. Shlaen, and D. Johrendt, The van der Waals ferromagnets $Fe_{5-\delta}GeTe_2$ and $Fe_{5-\delta-x}Ni_xGeTe_2$—crystal structure, stacking faults, and magnetic properties, Z. Anorg. Allg. Chem. **644**, 1923 (2018).
[36] X. Chen, Y.-T. Shao, R. Chen, S. Susarla, T. Hogan, Y. He, H. Zhang, S. Wang, J. Yao, P. Ercius, D. A. Muller, R. Ramesh, and R. J. Birgeneau, Pervasive beyond room-temperature ferromagnetism in a doped van der Waals magnet, Phys. Rev. Lett. **128**, 217203 (2022).
[37] X. Chen, E. Schierle, Y. He, M. Vranas, J. W. Freeland, J. L. McChesney, R. Ramesh, R. J. Birgeneau, and A. Frano, Antiferromagnetic order in co-doped Fe_5GeTe_2 probed by resonant magnetic x-ray scattering, Phys. Rev. Mater. **6**, 094404 (2022).
[38] X. Chen, W. Tian, Y. He, H. Zhang, T. L. Werner, S. Lapidus, J. P. C. Ruff, R. Ramesh, and R. J. Birgeneau, Thermal cycling induced alteration of the stacking order and spin-flip in the room temperature van der Waals magnet Fe_5GeTe_2, Phys. Rev. Mater. **7**, 044411 (2023).
[39] G. Zhang, F. Guo, H. Wu, X. Wen, L. Yang, W. Jin, W. Zhang, and H. Chang, Above-room-temperature strong intrinsic ferromagnetism in 2D van der Waals Fe_3GaTe_2 with large perpendicular magnetic anisotropy, Nat. Commun. **13**, 5067 (2022).
[40] S. Bao, W. Wang, Y. Shangguan, Z. Cai, Z.-Y. Dong, Z. Huang, W. Si, Z. Ma, R. Kajimoto, K. Ikeuchi, S.-I. Yano, S.-L. Yu, X. Wan, J.-X. Li, and J. Wen, Neutron spectroscopy evidence on the dual nature of magnetic excitations in a van der Waals

metallic ferromagnet $Fe_{2.72}GeTe_2$, Phys. Rev. X **12**, 011022 (2022).

[41] Y. Zhang, H. Lu, X. Zhu, S. Tan, W. Feng, Q. Liu, W. Zhang, Q. Chen, Y. Liu, X. Luo, D. Xie, L. Luo, Z. Zhang, and X. Lai, Emergence of Kondo lattice behavior in a van der Waals itinerant ferromagnet Fe_3GeTe_2, Sci. Adv. **4**, eaao6791 (2018).

[42] J.-X. Zhu, M. Janoschek, D. S. Chaves, J. C. Cezar, T. Durakiewicz, F. Ronning, Y. Sassa, M. Mansson, B. L. Scott, N. Wakeham, E. D. Bauer, and J. D. Thompson, Electronic correlation and magnetism in the ferromagnetic metal Fe_3GeTe_2, Phys. Rev. B **93**, 144404 (2016).

[43] X. Bai, F. Lechermann, Y. Liu, Y. Cheng, A. I. Kolesnikov, F. Ye, T. J. Williams, S. Chi, T. Hong, G. E. Granroth, A. F. May, and S. Calder, Antiferromagnetic fluctuations and orbital-selective Mott transition in the van der Waals ferromagnet $Fe_{3-x}GeTe_2$, Phys. Rev. B **106**, 184105 (2022).

[44] T. J. Kim, S. Ryee, and M. J. Han, Fe_3GeTe_2: a site-differentiated Hund metal, npj Comput. Mater. **8**, 245 (2022).

[45] X. Li, M. Zhu, Y. Wang, F. Zheng, J. Dong, Y. Zhou, L. You, and J. Zhang, Tremendous tunneling magnetoresistance effects based on van der Waals room-temperature ferromagnet Fe_3GaTe_2 with highly spin-polarized fermi surfaces, Appl. Phys. Lett. **122**, 082404 (2023).

[46] W. Jin, G. Zhang, H. Wu, L. Yang, W. Zhang, and H. Chang, Room-temperature spin-valve devices based on $Fe_3GaTe_2/MoS_2/Fe_3GaTe_2$ 2D van der Waals heterojunctions, Nanoscale **15**, 5371 (2023).

[47] W. Jin, G. Zhang, H. Wu, L. Yang, W. Zhang, and H. Chang, Room-temperature and tunable tunneling magnetoresistance in Fe_3GaTe_2-based 2D van der Waals heterojunctions, ACS Appl. Mater. Interfaces **15**, 36519 (2023).

[48] W. Li, W. Zhu, G. Zhang, H. Wu, S. Zhu, R. Li, E. Zhang, X. Zhang, Y. Deng, J. Zhang, L. Zhao, H. Chang, and K. Wang, Room-temperature van der Waals 2D ferromagnet switching by spin-orbit torques, Adv. Mater. **35**, 2303688 (2023).

[49] See Supplemental Material at http://link.aps.org/supplemental/10.1103/PhysRevB.109.104410 for detailed temperature-dependent x-ray absorption spectroscopy and x-ray magnetic circular dichroism; additional DFT calculations; additional photon energy-dependent ARPES data; additional temperature-dependent ARPES data; and comparison of the DFT and the ARPES data. It also contains Ref. [39].

[50] P. Blaha, K. Schwarz, F. Tran, R. Laskowski, G. K. H. Madsen, and L. D. Marks, WIEN2k: An APW+lo program for calculating the properties of solids, J. Chem. Phys. **152**, 074101 (2020).

[51] J. P. Perdew, K. Burke, and M. Ernzerhof, Generalized gradient approximation made simple, Phys. Rev. Lett. **77**, 3865 (1996).

[52] K. Kim, J. Seo, E. Lee, K.-T. Ko, B. S. Kim, B. G. Jang, J. M. Ok, J. Lee, Y. J. Jo, W. Kang, J. H. Shim, C. Kim, H. W. Yeom, B. I. Min, B.-J. Yang, and J. S. Kim, Large anomalous hall current induced by topological nodal lines in a ferromagnetic van der Waals semimetal, Nat. Mater. **17**, 794 (2018).

[53] H. Wu, A. M. Hallas, X. Cai, J. Huang, J. S. Oh, V. Loganathan, A. Weiland, G. T. McCandless, J. Y. Chan, S.-K. Mo, D. Lu, M. Hashimoto, J. Denlinger, R. J. Birgeneau, A. H. Nevidomskyy, G. Li, E. Morosan, and M. Yi, Nonsymmorphic symmetry-protected band crossings in a square-net metal $PtPb_4$, npj Quantum Mater. **7**, 31 (2022).

[54] A. I. Lichtenstein, M. I. Katsnelson, and G. Kotliar, Finite-temperature magnetism of transition metals: An *ab initio* dynamical mean-field theory, Phys. Rev. Lett. **87**, 067205 (2001).

[55] J. Sánchez-Barriga, J. Fink, V. Boni, I. Di Marco, J. Braun, J. Minár, A. Varykhalov, O. Rader, V. Bellini, F. Manghi, H. Ebert, M. I. Katsnelson, A. I. Lichtenstein, O. Eriksson, W. Eberhardt, and H. A. Dürr, Strength of correlation effects in the electronic structure of iron, Phys. Rev. Lett. **103**, 267203 (2009).

[56] D. E. Shai, C. Adamo, D. W. Shen, C. M. Brooks, J. W. Harter, E. J. Monkman, B. Burganov, D. G. Schlom, and K. M. Shen, Quasiparticle mass enhancement and temperature dependence of the electronic structure of ferromagnetic $SrRuO_3$ thin films, Phys. Rev. Lett. **110**, 087004 (2013).

[57] S. Hahn, B. Sohn, M. Kim, J. R. Kim, S. Huh, Y. Kim, W. Kyung, M. Kim, D. Kim, Y. Kim, T. W. Noh, J. H. Shim, and C. Kim, Observation of spin-dependent dual ferromagnetism in perovskite ruthenates, Phys. Rev. Lett. **127**, 256401 (2021).

[58] A. Grechnev, I. Di Marco, M. I. Katsnelson, A. I. Lichtenstein, J. Wills, and O. Eriksson, Theory of bulk and surface quasiparticle spectra for Fe, Co, and Ni, Phys. Rev. B **76**, 035107 (2007).

[59] J. Huang, Z. Wang, H. Pang, H. Wu, H. Cao, S.-K. Mo, A. Rustagi, A. F. Kemper, M. Wang, M. Yi, and R. J. Birgeneau, Flat-band-induced itinerant ferromagnetism in $RbCo_2Se_2$, Phys. Rev. B **103**, 165105 (2021).

[60] J. Hubbard, The magnetism of iron, Phys. Rev. B **19**, 2626 (1979).

[61] I. M. Billas, A. Châtelain, and W. A. de Heer, Magnetism from the atom to the bulk in iron, cobalt, and nickel clusters, Science **265**, 1682 (1994).

[62] Y. Fang, H. Zhang, D. Wang, G. Yang, Y. Wu, P. Li, Z. Xiao, T. Lin, H. Zheng, X.-L. Li, H.-H. Wang, F. Rodolakis, Y. Song, Y. Wang, C. Cao, and Y. Liu, Quasiparticle characteristics of the weakly ferromagnetic Hund metal MnSi, Phys. Rev. B **106**, 075117 (2022).

[63] Z. Jin, Y. Li, Z. Hu, B. Hu, Y. Liu, K. Iida, K. Kamazawa, M. B. Stone, A. I. Kolesnikov, D. L. Abernathy, X. Zhang, H. Chen, Y. Wang, C. Fang, B. Wu, I. A. Zaliznyak, J. M. Tranquada, and Y. Li, Magnetic molecular orbitals in MnSi, Sci. Adv. **9**, eadd5239 (2023).